Observation and Analysis of the Quality Factor Variation behavior in a Monolithic Fused Silica Cylindrical Resonator

Yao Pan, Tianliang Qu*, Dongya Wang, Suyong Wu, Jianping Liu, Zhongqi Tan, Kaiyong Yang, Hui Luo*

College of Optoelectronic Science and Engineering, National University of Defense Technology, Deya 109, 410073 Changsha, CHINA.

Emails: yaomeredithpan@hotmail.com (Y.P.); mywangdongya@126.com (D.W.); sywu2001@163.com (S.W.); l_jianp@sina.com (J.L.); zhqitan@sina.com (Z. T.); yky208@nudt.edu.cn (K.Y.)

* Correspondence:

Prof. Tianliang Qu

Email: qutianliang@nudt.edu.cn

Tel.: +86-731-8457-4730

Fax: +86-731-8457-3747

Prof. Hui Luo

Email: luohui.luo@163.com

Tel.: +86-731-8457-3741

Fax: +86-731-8457-3747

1. Introduction

Coriolis vibratory gyroscopes (CVG) are one of the most commonly used and fastest developing type of gyroscopes in inertial navigation systems. The well-known hemispherical resonator gyroscope (HRG) is considered the only technology capable of several decades' operation without failure in space [1, 2]. Quality factor and its mismatch are vital parameters of the resonator which determine the noise level and sensitivity of the CVG. Using fused silica material, the Q factor of the HRG achieved over 25 million [2], which is one of the reasons why HRG is the only kind of CVG that has achieved navigation-grade performance. Despite their remarkable advantages, HRGs demand rather complicated manufacturing process and extremely high cost.

Cylindrical resonator gyroscope (CRG) is considered a lower-cost and easier-manufacturing variant while preserving medium accuracy performance and the inherent rugged nature. It also shares with HRG advantages of instant start-up capability, considerable vibration and shock resistance and long lifespan, etc.; therefore it is highly competitive in medium accuracy market when size, weight, power consumption and cost are comprehensively considered. A number of cylindrical resonator gyroscopes have been proposed [3-8], with Q factors ranging from several thousands to nearly one million. While efforts have been focused on the Q factor

improvement of fused silica material and resonators [7, 9-11] and the analysis of loss

mechanisms [5, 8, 12-14], research on Q factor asymmetry is rare despite the fact that

it is a major source of errors for Coriolis vibratory gyroscopes [15-19]. In his

well-recognized work [15], D. D. Lynch briefly described the drift mechanism of

asymmetric damping (i.e., asymmetric Q factors around the azimuth axis of the

resonator) for hemispherical resonator gyroscopes. He also included the asymmetric

damping and defined principle damping axes in his widely-applied generic model of

Coriolis vibratory gyroscopes [16]. Y. K. Zhbanov has considered methods to suppress

drift caused by Q factor asymmetry [17], and M. Shatalov and C. Coetzee gave a

detailed electro-mechanical model of HRGs, showing that drift caused by Q-factor

difference could be compensated by proper controlling the discrete parametric drive

functions [18]. These works stand significant theoretical and practical value on CVG

control, however, they did not address the measurement of Q factor asymmetry, nor

did they systematically analyze the Q variation behavior of resonators. As for the

experimental measurement of Q factor variation, X. Xi et al. briefly mentioned the

circumferential change of Q factors [5]. However, they conclude this change as a

cosine function, and they did not further explain the reason for this phenomenon. As

the Q factor asymmetry of the resonator is detrimental to gyro performance, it is of

great importance to measure and study the Q factor asymmetry in addition to enhancing Q factor of resonators.

The initiative of this study was to characterize the Q factor and its asymmetry of the cylindrical resonator reported in [7]. During characterization we discovered the circumferential Q variation when the resonator was excited at one direction and measured at different directions. In this paper, we first briefly introduced the basics of the cylindrical resonator, and demonstrated our Q factor measurement procedure based on the non-contact method using an acoustic source for excitation and a laser Doppler vibrometer for detection. We then presented our discovery that the Q factor varies periodically around the azimuth axis of the resonator. Based on the two-dimensional mass-spring model, we numerically simulated the measurement procedure. Numerical calculations were consistent with experimental results, suggesting the Q factor variation behavior is due to the existence of frequency mismatch and Q asymmetry, and the misalignment of excitation direction with principle axes. We concluded that for each detection point, the vibration is the superposition of two eigen-modes, and fitting with a one-dimensional oscillator would result in repetitive errors.

2. Basic Concepts and Theories

2.1. Resonator Structure and Operational Principle

Our resonator structure is based on the cylindrical shell resonator first reported by V. V. Chikovani et al. [8, 9], but is the first monolithic fused silica variant [7]. As shown in Fig. 1(a), the main sensing element of the resonator is the resonant shell, the thickness of which was carefully designed to ensure the resonator has an appropriate wineglass mode frequency and an acceptable sensitivity. The vibration-conducting shell should be as thin as manufacturing process can provide, so as to better conduct the vibration between resonant shell and the bottom plate, where the sensing element is usually attached. The holes of the bottom plate can decrease the stiffness of the bottom plate. In the ideal case, the vibration modes are spatially orthogonal (in the case of n=2 wineglass modes, their angular positions are 45° relative to each other) and have equal eigen-frequencies. Each direction would be equivalent for excitation because the vibration modes have indeterminate angular positions around the axis of symmetry. The wineglass modes were shown with FEM simulation figures in Fig 1(b).
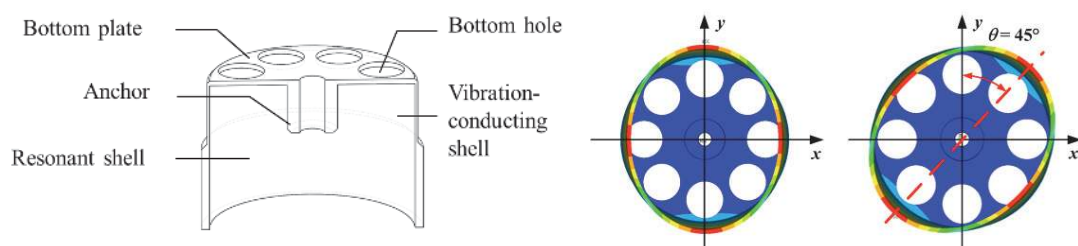

Fig. 1. (a) The structure of the monolithic fused silica cylindrical resonator. **(b)** FEM simulation of the wineglass modes.

The operational principle of the cylindrical resonator gyroscope is well understood [16, 19-23]. The cylindrical resonator is excited at a constant amplitude in n=2 wineglass mode, as shown in Fig. 2(a), which is often referred to as the drive mode or the primary mode. The driving mechanism can be piezo-electric, electrostatic, electromagnetic, etc. The Coriolis force due to external rotation gives rise to the response mode (or the secondary mode), which is ideally at 45 degrees relative to the primary mode. The amplitude of the secondary mode is proportional to the external angular rate. The cylindrical resonator gyroscope usually works in the force-to-rebalance mode, in which the angular rate is proportional to the force applied to null the secondary mode arisen from external rotation [24].

However, imperfections are inevitable in real devices due to material anisotropy and manufacturing errors. These imperfections cause frequency split as well as Q factor asymmetry, which result in two sets of principle axes, the frequency axes and the damping axes. These two sets principle axes often do not coincide with each other [15]. As shown in Fig. 2(b), each set of axes contains two axes, which lie 45° relative to each other. The angular positions of these axes are defined by θ_k and θ_c in respect to the x direction in an anti-clockwise manner. To illustrate, we assume that the two eigen-frequencies are f_1 and f_2, respectively. The angular position of f_1 axis is θ_k

anti-clockwise in respect to *x*, and the angular position of f_2 axis is 45° anti-clockwise

from f_1 axis. The damping axes are similarly defined, with two eigen-Q factors denoted

by Q_1 and Q_2, respectively. The frequency mismatch and the Q factor asymmetry are

defined as $\Delta f=f_1-f_2$ and $\Delta Q=Q_1-Q_2$, respectively.

(a)

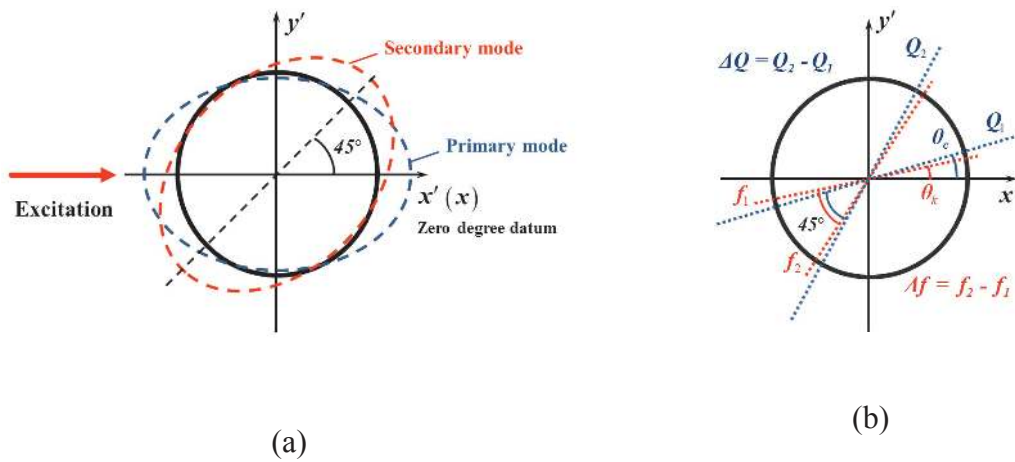(b)

Fig. 2. Schematic of: (**a**) the vibration mode of an ideal cylindrical resonator; (**b**) the

definition of coordinates and parameters of a practical imperfect cylindrical resonator.

2.2. Q factor

For a cylindrical resonator, a higher Q factor means higher sensitivity and lower

noise level. Q factor is commonly used to express energy dissipations in resonant

systems, which is defined by energy stored in the system divided by energy dissipated

per resonant cycle as in

$$Q=2\pi \times \frac{E_{total}}{\Delta E} \tag{1}$$

o

Where E_{total} is the total stored energy, which is the sum of the kinetic and potential energies at some point of time, and $\varDelta E$ is the dissipated energy per resonant cycle, which is related to various damping mechanism: external loss including air damping (Q_{air}), support loss (Q_{sup}); internal loss of the resonator and material including surface loss (Q_{surf}) and thermal elastic damping (Q_{TED}), etc. The total Q factor can also be described as

$$\frac{1}{Q} = \frac{1}{Q_{air}} + \frac{1}{Q_{sup}} + \frac{1}{Q_{surf}} + \frac{1}{Q_{TED}} + \frac{1}{Q_{others}} \tag{2}$$

As different loss mechanisms usually vary in orders of magnitude, the total loss is determined by the largest loss. Resonators with different sizes, structures and materials have different dominant loss mechanisms [5, 7, 8]. As our experiments were performed under atmospheric pressure, the setting loss in this case is air damping, which restricted the Q factor of our resonators to ~10^4 [7].

In experiment, the following definition is usually used for high values of Q

$$Q = \frac{f_r}{\varDelta f} \tag{3}$$

Where f_r is the resonant frequency and $\varDelta f$ is the 3-dB bandwidth of the resonant peak [25]. In the experimental procedure based on Equation (3), the amplitude frequency response (AFR) is used to calculate the Q factor of the resonator, thus the procedure is often referred to as the AFR method. For even higher Q factor (up to 10^5), the

ring-down time τ (when the vibration amplitude attenuate to *1/e* the initial value) was measured and the Q factor was calculated by $Q=\pi f_r \tau$.

3. Experiment

3.1. Experimental procedure

In Q factor studies it is important to measure the Q factor efficiently and accurately, therefore the excitation and detection system should be carefully designed. In previous studies, the excitation methods were mostly with contact, among which piezoelectric actuators were most commonly used to excite samples without metal coating [26-28]. As fused silica is brittle material, the contact may induce defect to the surface of the resonator, decreasing Q factor and increasing anisotropy. Better solution is to use electrostatic excitation as in Ref. [27] and [29], however, the design of the measurement system is relatively complex. Some researchers have proposed a simple acoustic method to excite and measure resonators [30, 31], which is convenient, low-cost and has reasonable accuracy in air. However, the distances between microphone sensors and the resonator rim may contain inaccuracy, and there is likely aerial crosstalk between microphones. This inspired us to combine acoustic excitation and laser Doppler vibrometry for measurement of Q factors in moderate vacuum [7]. Our proposed method is fast and convenient for preliminary measurement of resonator

characteristics, including Q factor, Q factor asymmetry, vibration mode frequency and frequency mismatch, thus is useful in initial screening of resonators. In addition, when air pressure is smaller, the air damping decreases and the effect of various treatments on Q can be better assessed.

The experimental setup is shown in Fig. 3. They were placed on an optical table to avoid environmental vibration. The rigid stem of the resonator was clamped with our designed fixture and together they were mounted on a rotary table. The rotary table was used to adjust the excitation angle. The resonator was excited by an acoustic source to the n=2 wineglass mode and its vibration detected by a Polytec laser Doppler vibrometer, which enabled non-contact characterization, avoiding possible surface damaging by contacting or extra damping by attaching exciting elements. In this study, we measured the Q factor by measuring the AFR characteristics of the resonator bottom, and the resonant data was processed by the Polytec software, which was essentially using equation (3) to calculate Q.
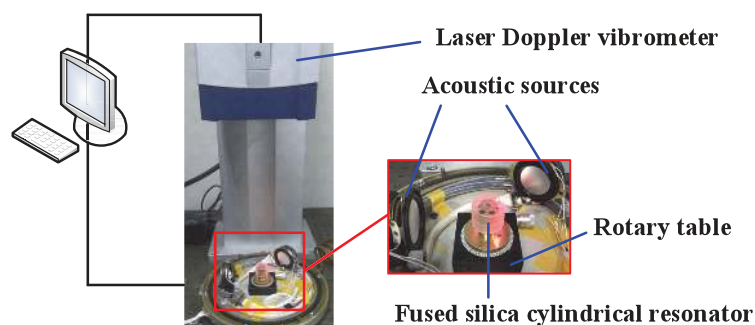
Fig. 3. The experimental setup. The acoustic source excites the cylindrical resonator to the n=2 wineglass mode, and the laser Doppler vibrometer acquires the vibration information, which is then processed by the Polytec software. A rotary table was used to adjust the excitation angle.

The measurements were performed according to the following steps. First, we defined 72 points at the rim of the resonator bottom, the center of which coincided with the resonator center; hence the angular interval between adjacent measurement points is 5 degrees. The excitation direction is aligned with the axis of symmetry, as shown in Fig. 4(a). Second, we measured the AFR of the resonator in a relatively large frequency range to find the resonant frequency, and then measured the AFR in an 8-Hz frequency range to determine the frequency more accurately. Next, we used sine signals to excite the resonator at the resonant frequency, and scanned the defined points to see the resonant mode. Then we slightly adjusted the angle of the resonator and repeated the last step until the node vibration was minimum, when the excitation direction was roughly aligned with the principle low frequency axis, i.e., $\theta_k \approx 0°$. Then we set one antinode of the vibration pattern as the zero-degree datum direction, at which $\theta_{d_1} = 0°$, as shown in Fig. 4(b). Then the resonator was kept still, and the AFRs of the 72 defined points with $\theta_{d_i} = \left[(i-1) \times 5\right]°$ were measured one by one, each

point being swept in an 8-Hz frequency range. The AFRs of different testing points were subsequently fitted by the Polytec software in a 0.4-Hz range and the Q factors were calculated, as shown in Fig. 4(c). The velocity at the resonant frequency was also recorded to shown the vibration pattern. Then the resonator were turned 5⁰, 10⁰ and 15 ⁰ clockwise using the turntable, i.e., θ_k=5⁰, 10⁰ and 15⁰, and the measurement procedures were repeated for three times.

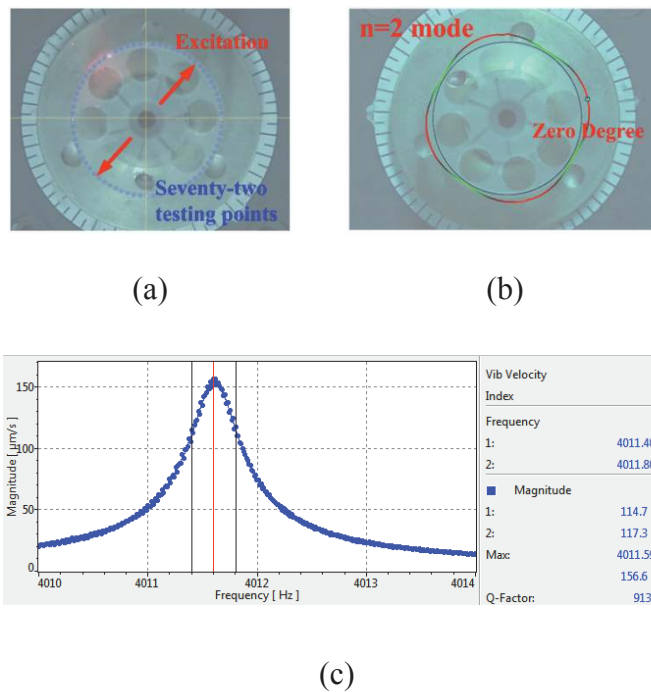(a)   (b)

(c)

Fig. 4. The measurement procedures. **(a)** Seventy-two measurement points were defined equi-angularly on the bottom plate of the resonator, and the excitation was aligned with principle frequency axis. **(b)** The mode shape was identified, and the antinode of the vibration sought out and defined as the zero-degree datum. **(c)** The

AFR of each measurement point was fitted in the Polytec software and the Q factor was calculated.

3.2. Results

The vibration patterns were shown in Fig. 5(a), which showed that the resonator vibrated at the typical wineglass mode. As the excitation direction deviated from the principle low frequency axis, the resonant amplitudes decreased and the vibration pattern drifted toward the direction of the principle axes. The measured frequencies were shown in Fig. 5(b). When excited at 0°, the measured frequencies showed a clear temperature drift (Previous experiments had shown the frequency of the resonator varied at 0.401Hz/℃[32]). After the stabilization of laboratory temperature, the measured frequency of 5°, 10°, and 15° showed a similar decreasing trend from antinodes to nodes. When the detection points were near the principle high frequency axis, the low frequency cannot be measured. Then the low frequency mode reappeared with a slightly higher frequency and repeated the variation pattern.

The corresponding circumferential variations of Q factors were shown in Fig. 5(c)(d). The Q factors varied significantly and repetitively around the azimuth axis, and the variation pattern repeated every 90 degrees. The Q factors became more unstable as the increase of the angle between excitation and principle axes, and showed

an increase tendency from the vibration nodes to antinodes. The Q factors continued

increasing until reaching local maximum, starting from which Q factors dropped
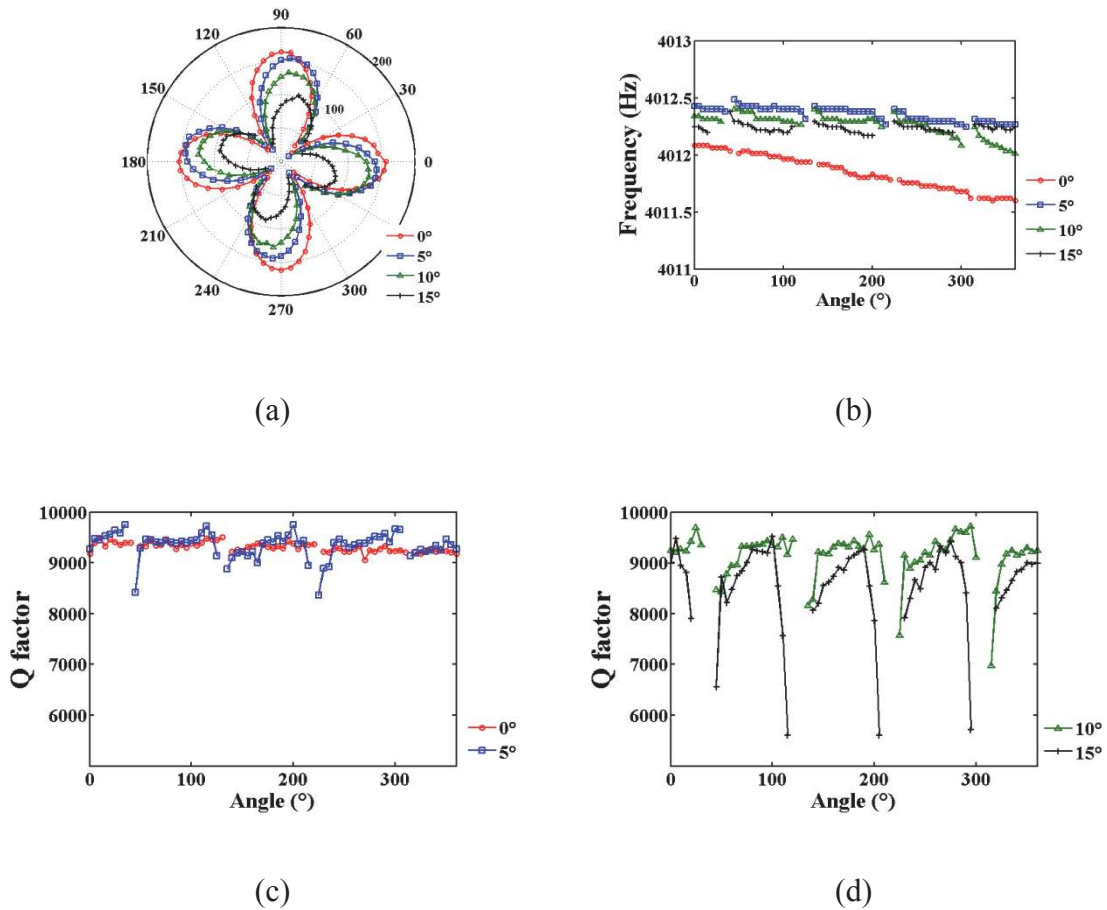
dramatically.

(a)   (b)

(c)   (d)

Fig. 5. Experimental results. **(a)** The vibration patterns showed the resonator

vibrated at n=2 wineglass mode, and the vibration had a tendency to drift toward the

principle axes. **(b)** The circumferential frequency variation. **(c)** The circumferential Q

factor variation when excited at 0° and 5°. **(d)** The circumferential Q factor variation

when excited at 10° and 15°.

4. Analysis

We analyzed the Q variation around the azimuth axis based on the two-dimensional mass-spring model. In the configurative space of the mass-spring system, assuming that x direction and y direction are aligned with the excitation (primary mode) and the detection (secondary mode) direction, respectively, as shown in Fig. 6.
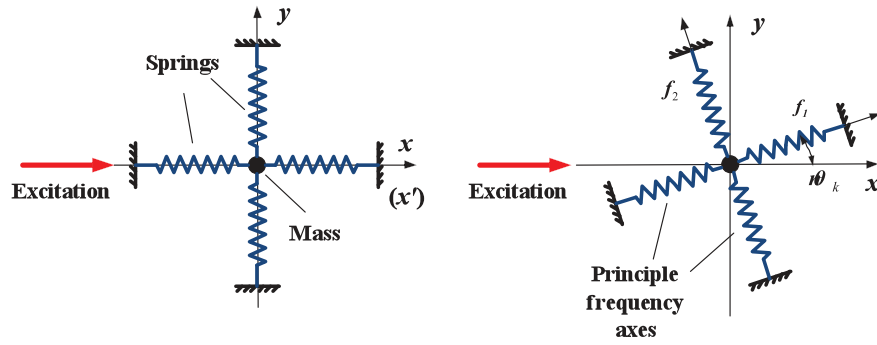

Fig. 6. Schematic of the two-dimensional oscillator model.

Assuming that Δf and ΔQ are very small, and the Q factor is large enough. The resonator is excited along the x axis, and the excitation force along the y axis is zero; therefore the dynamic equations for the resonator are [16]:

$$\begin{cases} \ddot{x} + c_{11}\dot{x} + k_{11}x = F_0 e^{i\omega t} \\ \ddot{y} + c_{21}\dot{x} + c_{22}\dot{y} + k_{21}x + k_{22}y = 0 \end{cases} \tag{4}$$

Where $\omega=2\pi f$ is the frequency of the excitation force, and other parameters in equation (4) are given in the Appendix A. In this equation, the energy coupling from direction y to x is neglected because according to above assumptions the coupling

should be small compared with the excitation force. Note that θ_k and θ_c are defined in the physical space (x', y') of the cylindrical resonator; therefore, it corresponds to $n\theta_k$ and $n\theta_c$ in the configuration space (x, y), respectively, where $n=2$ is the number of nodal lines for wineglass mode. Note that the vibration of the primary mode at the x direction is coupled to the secondary mode at the y direction through c_{21}, the coefficient including the effect of Q factor asymmetry (ΔQ and θ_c), and k_{21}, the coefficient including the effect of frequency mismatch (Δf and θ_k).

Assuming that the steady state response (normalized by $1/F_0$) of the primary oscillation mode is

$$x = X(\omega)e^{i\omega t} \tag{5}$$

Where $\omega=2\pi f$ is the angular frequency, and the complex frequency response of the primary mode is

$$X(\omega) = \frac{1}{k_{11} - \omega^2 + ic_{11}\omega} \tag{6}$$

Therefore, the amplitude frequency response (AFR) and the phase frequency response (PFR) are:

$$\begin{cases} A(\omega) = \dfrac{1}{\sqrt{\left(k_{11} - \omega^2\right)^2 + c_{11}^2\omega^2}} \\ \Phi(\omega) = \arctan(\dfrac{-c_{11}\omega}{k_{11} - \omega^2}) \end{cases} \tag{7}$$

Similarly, assuming that the steady state response of the secondary oscillation mode is

$$y = Y(\omega)e^{i\omega t} \tag{8}$$

Substituting (8) into the second equation of (3), the complex frequency response of the secondary mode is:

$$
\begin{aligned}
Y(\omega) &= \frac{k_{21} - ic_{21}\omega}{k_{22} - \omega^2 + ic_{22}\omega} X \\
&= \frac{k_{21} - ic_{21}\omega}{\left(k_{22} - \omega^2 + ic_{22}\omega\right)\left(k_{11} - \omega^2 + ic_{11}\omega\right)}
\end{aligned}
\tag{9}
$$

Then the AFR and the PFR of the secondary oscillation are:

$$
\left\{
\begin{aligned}
B(\omega) &= \sqrt{\frac{k_{21}^2 + c_{21}^2\omega^2}{\left[\left(k_{11} - \omega^2\right)^2 + c_{11}^2\omega^2\right]\left[\left(k_{22} - \omega^2\right)^2 + c_{22}^2\omega^2\right]}} \\
\Theta(\omega) &= \arctan\left(-\frac{\begin{array}{l} k_{21}\omega\left[c_{11}\left(k_{22} - \omega^2\right) + c_{22}\left(k_{11} - \omega^2\right)\right] \\ +c_{21}\omega\left[\left(k_{22} - \omega^2\right)\left(k_{11} - \omega^2\right) - c_{11}c_{22}\omega^2\right] \end{array}}{\begin{array}{l} k_{21}\left[\left(k_{22} - \omega^2\right)\left(k_{11} - \omega^2\right) - c_{11}c_{22}\omega^2\right] \\ -c_{21}\omega^2\left[c_{11}\left(k_{22} - \omega^2\right) + c_{22}\left(k_{11} - \omega^2\right)\right] \end{array}}\right)
\end{aligned}
\right.
\tag{10}
$$

According to the principle of mode superposition, the point at a detection angle of θ_{d_i} should have a complex response of

$$
\begin{aligned}
Z(\omega) &= X(\omega)\cos 2\theta_{d_i} + Y(\omega)\sin 2\theta_{d_i} \\
&= \frac{\left[\left(k_{22} - \omega^2\right)\cos 2\theta_{d_i} + k_{21}\sin 2\theta_{d_i}\right] + i\omega\left(c_{22}\cos 2\theta_{d_i} - c_{21}\sin 2\theta_{d_i}\right)}{\left(k_{11} - \omega^2 + ic_{11}\omega\right)\left(k_{22} - \omega^2 + ic_{22}\omega\right)} \\
&= CB_i(\omega)e^{i\omega\Psi_i(\omega)}
\end{aligned}
\tag{11}
$$

From equation (11) (11)the AFR $CB_i(\omega)$ of different detection directions can be calculated, where i=1,2,…72, and the detection angle is denoted as in $\theta_{d_i} = \left[(i-1)\times 5\right]^\circ$. The calculations of AFR and PFR are given in the Appendix B, where both $CB_i(\omega)$ and $\Psi_i(\omega)$ include $c_{11,}\, c_{21,}\, c_{22}$ (related to Q_1, Q_2, ΔQ and θ_c) and k_{11}, k_{21}, k_{22} (related to f_1, f_2, Δf and θ_k). Therefore, the vibration of the point at θ_{d_i} would be essentially the superposition of the primary and secondary mode，the AFR $CB_i(\omega)$ of which was affected by the complex coupling of parameters of both eigen-modes.

We then numerically simulated the experimental process using Mathematica software. The parameters of the principle axes were measured to provide the input for the simulation. As the measurement was performed in air, and it only allowed us to determine the principle frequency axes, we assumed the principle damping axes coincide with the frequency axes [30]. The eigen-frequencies were measured as 4013.062Hz and 4011.538Hz, respectively, and the Q factor were 9421 and 8459, respectively. Then, we discretized the calculated $CB_i(\omega)$ to simulate the data collecting process in experiments, and then we used the single degree-of-freedom damped oscillator model to fit the data and calculate the Q factor, just as the fitting of experimental curve in the LDV software, as shown in Fig. 7. The fitting equation is

$$CB_i = \frac{A}{\sqrt{f^4 + f^2 f_2^2 \left(1/Q^2 - 2\right) + f_2^4}} \tag{12}$$

The discretized $CB_i(\omega)$ was used to the fitting process and the Q factors and frequencies for different numerical detection points were calculated. Here we also chose a data range of ±0.2 Hz near the resonant peak, fitting only the dominant mode, the similar process as in the experiment. As we excite near the f_2 principle axis, the f_2 mode dominates at most detection angles.
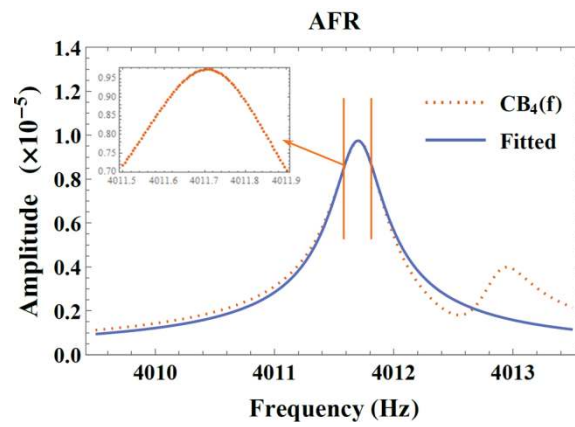

Fig. 7. The exemplification of data collecting and fitting processes. The calculated CB_4 was discretized and then fitted with a single degree-of-freedom damped oscillator model.
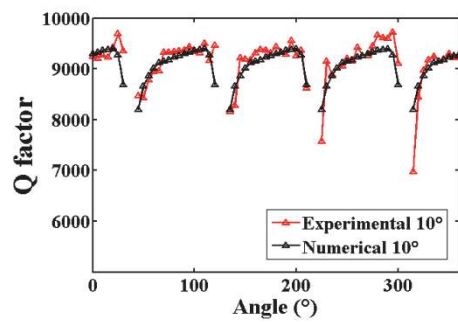
The Q factor for different detection directions was calculated and compared with experimental results, as shown in Fig. 8. The calculated variation patterns were in close agreement with experimental results, which repeat every 90°.
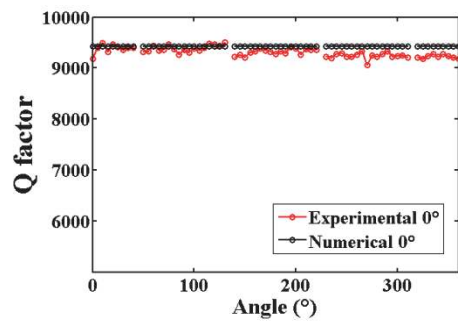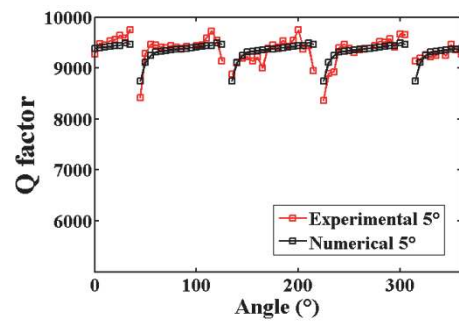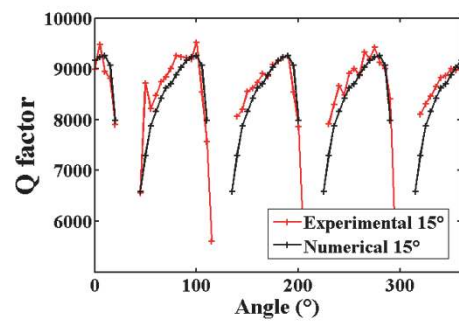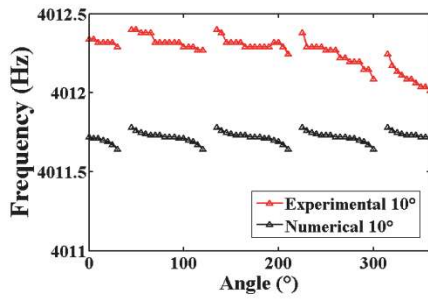
Fig. 8. The comparison between numerically simulated Q factors and measured Q factors, when resonator was excited at **(a)** 0°, **(b)** 5°, **(c)** 10°, and **(d)** 15°.

In addition, the numerically calculated frequencies also showed a variation pattern that was consistent with experimental results. As an example, the calculated frequencies when resonator was excited at 10° and 15° relative to the low frequency axis were depicted in Fig. 9.
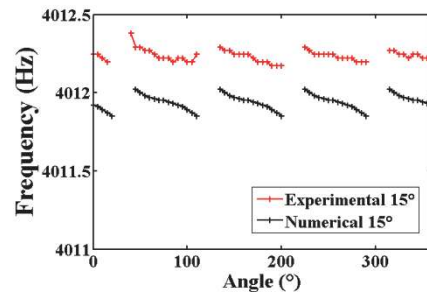
Fig. 9. The comparison between numerically simulated frequencies and measured frequencies, when resonator was excited at **(a)** 10° and **(b)** 15°.

The consistency between experimental results and numerical calculation confirmed that the characteristics of the cylindrical resonator can be simplified by a two-dimensional mass-spring system, and that the vibration at different angles of the cylindrical shell can indeed be simplified and represented by mode superposition. The Q variation and frequency deviation measured was caused by the coupling of two natural modes at different directions, which is affected by the frequencies and Q factors of both eigen-modes. When fitted by a single degree-of-freedom system equation, the vibration characteristics varied in a repetitive manner, which changes with the angle between excitation and principle axes. The more misaligned the excitation direction with principle axes, the more unstable both Q factors and frequencies become. As a result, measurement errors occur in the case of resonator characterization and drift errors occur in the case of vibratory gyroscopes.

Furthermore, the measurement results of 0°, 5°, 10° and 15° were compared statistically. Specifically, the measured data at 0° gave an average frequency of 4011.847 Hz for the 72 defined points, with a relative variation range of 32 ppm. The Q factors of the defined points ranged from 9056 to 9500. The circumferential average Q (Average Q 1) was 9311, and the circumferential variation of Q (QV 1) was 0.96%. The average Q at ±10° close to antinodes was 9294 and the corresponding variation of Q (QV 2) was 0.99%. The rest of data was analyzed similarly and results were listed in Table 1.

Table 1

Analysis and comparison of the experimental results with different excitation angles.

Excitation Degrees (°)	Average Frequency (Hz)	Frequency Variation (ppm)	Average Q 1	QV1	Average Q 2	QV2
0	4011.847	38	9311	0.97%	9294	0.99%
5	4012.358	15	9346	2.72%	9375	1.19%
10	4012.264	24	9143	5.07%	9295	0.90%
15	4012.234	9	8552	10.2%	9011	1.8%

As shown in Fig. 5 and Table 1, as the excitation deviates from the principle axes, the average Q factor decreases, and the variation of Q factor increases, especially near the vibration nodes. Because the vibration has a tendency to drift toward principle axes, as is shown in Fig. 5(a), failing to excite the resonator along the principle directions will result in instabilities in both Q factor and frequency, introducing measurement errors. This phenomenon could also explain the gyro drift when the excitation and detection elements are misaligned. Therefore, when characterizing resonators and assembling gyroscopes, it is preferred to align the excitation with principle axes, and to keep the detection orthogonal with excitation (e.g., 90 in the case of n=2 wineglass mode).

However, it is worth mentioning that the Q factors near the vibration antinodes are relatively stable, therefore can be used as a parameter for preliminary resonator monitoring. As shown in Table 1, to measure antinode Q factor when excitation is within ±10° would cause measurement errors of no more than 3%, thus is a convenient and relatively accurate method for preliminary Q factor tests.

5. Conclusion

In this paper, we report that the Q factor varies periodically around the resonator's azimuth axis. The non-contact method of measuring the Q factor of the cylindrical

resonators was demonstrated, using an acoustic source for excitation and a laser Doppler vibrometer for detection, and we measured the resonator Q factor by the amplitude frequency response (AFR) method using the multi-point scanning measurement function of the LDV. The experimental results were in close agreement with our theoretical calculation. We demonstrated that as the excitation deviated from the principle frequency axes, the Q factor variation pattern changes regularly and the frequencies also changes with respect to detection angle. We showed that the nature of this Q variation was that, for each detection point, the vibration is the superposition of two eigen-modes, the AFR of which would be affected by the frequencies and Q factors of both eigen-modes. Therefore, fitting with a one-dimensional oscillator would result in repetitive errors. While Q factors of the vibration antinodes is relatively stable to be used as a parameter for preliminary monitoring of resonators, it is of great importance to align the excitation with principle axes to reduce errors when higher accuracy is demanded.

Acknowledgments

References

[1] D.M. Rozelle, The hemispherical resonator gyro: From wineglass to the planets, Adv. Astronaut. Sci. 134 (2009) 1157–1178.

[2] Anon., Northrop Grumman ' s Hemispherical Resonator Gyro Marks 30 Million Operating Hours in Space, (n.d.). http://www.globenewswire.com/newsarchive/noc/press/pages/news_releases.html?d=1 0120447 (accessed January 29, 2016).

[3] V. V. Chikovani, I.M. Okon, A.S. Barabashov, P. Tewksbury, A set of high accuracy low cost metallic resonator CVG, Rec. - IEEE PLANS, Position Locat. Navig. Symp. (2008) 238–243. doi:10.1109/PLANS.2008.4569975.

[4] V. V. Chikovani, Y.A. Yatsenko, A.S. Barabashov, P.I. Marusyk, E.O. Umakhanov, V.N. Taturin, Improved accuracy metallic resonator CVG, IEEE Aerosp. Electron. Syst. Mag. 24 (2009) 40–43. doi:10.1109/MAES.2009.5109952.

[5] X. Xi, X. Wu, Y. Zhang, X. Zhou, X. Wu, Y. Wu, A study on Q factor of the trimmed resonator for vibratory cupped gyroscopes, Sensors Actuators, A Phys. 218 (2014) 23–32. doi:10.1016/j.sna.2014.07.016.

[6] X. Xi, Y. Wu, X. Wu, Q. Luan, X. Wu, A Novel Combined Fused Silica Cylinder Shell Vibrating Gyroscope, 25 (2013) 323–339.

[7] Y. Pan, D. Wang, Y. Wang, J. Liu, S. Wu, T. Qu, K. Yang, H. Luo, Monolithic Cylindrical Fused Silica Resonators with High Q Factors, Sensors. 16 (2016) 1185. doi:10.3390/s16081185.

[8] D. Saito, C. Yang, A. Heidari, H. Najar, L. Lin, D.A. Horsley, Microcrystalline diamond cylindrical resonators with quality-factor up to 0.5 million, Appl. Phys. Lett. 108 (2016) 0–5. doi:10.1063/1.4939622.

[9] A. Ageev, B.C. Palmer, A. De Felice, S.D. Penn, P.R. Saulson, Very high quality factor measured in annealed fused silica, Class. Quantum Gravity. 21 (2004) 3887–3892. doi:10.1088/0264-9381/21/16/004.

[10] A. Duwel, R.N. Candler, T.W. Kenny, M. Varghese, Engineering MEMS Resonators With Low Thermoelastic Damping, 15 (2006) 1437–1445.

[11] J. Cho, T. Nagourney, A. Darvishian, B. Shiari, J. Woo, K. Najafi, Fused silica micro birdbath shell resonators with 1.2 million Q and 43 second decay time constant, Solid-State Sensors, Actuators Microsystems Conf. (Hilt. Head). (2014) 103–104.

[12] M.J. Ahamed, D. Senkal, A.M. Shkel, Effect of annealing on mechanical quality factor of fused quartz hemispherical resonator, 2014 Int. Symp. Inert. Sensors Syst. (2014) 1–4. doi:10.1109/ISISS.2014.6782512.

[13] B.S. Lunin, S.N. Torbin, On the mechanism of acoustic losses in the hydroxylated surface layer of silica glass, Moscow Univ. Chem. Bull. 56 (2001) 19–22.

[14] Y. Xi, Xiang and Wu, Xuezhong and Wu, Yulie and Zhang, Modeling and analysis of mechanical Quality factor of the resonator for cylinder vibratory gyroscope, Chinese J. Mech. Eng. (2016) 1–10.

[15] E.J. Loper, D.D. Lynch, Projected system performance based on recent HRG test results, IEEE/AIAA 5th Digit. Avion. Syst. Conf. (1983) 18.

[16] D.D. Lynch, Vibratory Gyro Analysis by the Method of Averaging, 2nd SAINT Petersbg. Int. Conf. GYROSCOPIC Technol. Navig. Part 1. (1995) 26–34.

[17] Y.K. Zhbanov, Amplitude control contour in a hemispherical resonator gyro with automatic compensation for difference in Q-factors, Mech. Solids. 43 (2008) 328–332. doi:10.3103/S0025654408030035.

[18] M. Shatalov, C. Coetzee, S. Joubert, Dynamics of a rotating and vibrating thin hemispherical shell with mass and damping imperfections and parametrically driven by discrete electrodes, in: 16th Saint Petersbg. Int. Conf. Integr. Navig. Syst. ICINS 2009 - Proc., 2009: pp. 120–127. doi:10.1134/s2075108711010093.

[19] V.A. Matveev, B.S. Lunin, M.A. Basarb, Solid-State Gyroscope Navigation System, 1st ed., Harbin Institute of Technology Press, Harbin, China, 2013.

[20] P.W. Loveday, C.A. Rogers, Free vibration of elastically supported thin cylinders including gyroscopic effects, J. Sound Vib. 217 (1998) 547–562. doi:10.1006/jsvi.1998.1765.

[21] P.W. Loveday, C.A. Rogers, Modification of piezoelectric vibratory gyroscope resonator parameters by feedback control, IEEE Trans. Ultrason. Ferroelectr. Freq. Control. 45 (1998) 1211–1215. doi:10.1109/58.726445.

[22] P.W. Loveday, Analysis and Compensation of Imperfection Effects In Piezoelectric Vibratory Gyroscopes, Mech. Eng. Ph.D (1999) 147.

[23] P.W. Loveday, C. a. Rogers, The Influence of Control System Design on the Performance of Vibratory Gyroscopes, J. Sound Vib. 255 (2002) 417–432. doi:10.1006/jsvi.2001.4163.

[24] Wang, X., Wu, W., Luo, B., Fang, Z., Li, Y., & Jiang, Q. (2011). Force to rebalance control of HRG and suppression of its errors on the basis of FPGA. Sensors, 11(12), 11761–11773. https://doi.org/10.3390/s111211761

[25] Y.Z. Liu, W.L. Chen, L.Q. Chen, Mechanics of Vibration, 1st ed., Higher Education Press, Beijing, China, 1998.

[26] W.J. Startin, M.A. Beilby, P.R. Saulson, Mechanical quality factors of fused silica resonators, Rev. Sci. Instrum. 69 (1998) 3681–3689. doi:10.1063/1.1149159.

[27] T. Uchiyama, T. Tomaru, M. Tobar, D. Tatsumi, S. Miyoki, M. Ohashi, K. Kuroda, T. Suzuki, N. Sato, T. Haruyama, others, Mechanical quality factor of a cryogenic sapphire test mass for gravitational wave detectors, Phys. Lett. A. 261 (1999) 5–11. doi:10.1016/S0375-9601(99)00563-0.

[28] K. Numata, G.B. Bianc, N. Ohishi, A. Sekiya, S. Otsuka, K. Kawabe, M. Ando, K. Tsubono, Measurement of the intrinsic mechanical loss of low-loss samples using a nodal support, Phys. Lett. Sect. A Gen. At. Solid State Phys. 276 (2000) 37–46. doi:10.1016/S0375-9601(00)00646-0.

[29] A. Ageev, B.C. Palmer, A. De Felice, S.D. Penn, P.R. Saulson, Very high quality factor measured in annealed fused silica, Class. Quantum Gravity. 21 (2004) 3887–3892. doi:10.1088/0264-9381/21/16/004.

[30] S.A. Rhee, Huinam and Park, Sangjin and Park, Junsung and Lee, Jongchan and Sarapuloff, Determination of Principal Axes of a Wineglass Using Acoustic Testing, in: Springer International Publishing, 2014: pp. 295–299.

[31] X. Xi, Y. Wu, Y. Zhang, X. Wu, Y. Zheng, X. Wu, A simple acoustic method for modal parameter measurement of the resonator for vibratory shell gyroscope, IEEE Sens. J. 14 (2014) 4069–4077. doi:10.1109/JSEN.2014.2332879.

[32] Y. Wu, Y. Pan, D. Wang, T. Qu, Y. Huang, The Study on Temperature Characteristics of a Monolithic Fused Silica Cylindrical Resonator, in: JIMEC-16, Atlantis Press, 2016: pp. 44–49. doi:10.2991/jimec-16.2016.9.

Appendix A

The parameters in Equation (3) are defined as follows:

$$f = \sqrt{\frac{f_1^2 + f_2^2}{2}}$$

$$c_{11} = \pi f \left[\left(\frac{1}{Q_1} + \frac{1}{Q_2} \right) + \left(\frac{1}{Q_1} - \frac{1}{Q_2} \right) \cos 4\theta_c \right]$$

$$c_{12} = \pi f \left(\frac{1}{Q_1} - \frac{1}{Q_2} \right) \sin 4\theta_c$$

$$c_{21} = \pi f \left(\frac{1}{Q_1} - \frac{1}{Q_2} \right) \sin 4\theta_c$$

$$c_{22} = \pi f \left[\left(\frac{1}{Q_1} + \frac{1}{Q_2} \right) - \left(\frac{1}{Q_1} - \frac{1}{Q_2} \right) \cos 4\theta_c \right]$$

$$k_{11} = 2\pi^2 \left[\left(f_1^2 + f_2^2 \right) - \left(f_1^2 - f_2^2 \right) \cos 4\theta_k \right]$$

$$k_{12} = -2\pi^2 \left(f_1^2 - f_2^2 \right) \sin 4\theta_k$$

$$k_{21} = -2\pi^2 \left(f_1^2 - f_2^2 \right) \sin 4\theta_k$$

$$k_{22} = 2\pi^2 \left[\left(f_1^2 + f_2^2 \right) + \left(f_1^2 - f_2^2 \right) \cos 4\theta_k \right]$$

$$\omega = 2\pi f$$

Where f_1 and f_2 are the two eigen-frequencies and Q_1 and Q_2 are the two eigen-Q

factors. The angular position of f_1 axis is denoted by θ_k, and the angular position of

Q_1 axis is denoted by θ_c.

Appendix B

The AFR and PFR of the detection point i is calculated as:

$$CB_i(\omega) = \sqrt{\frac{\left[\omega^2 \left(c_{21}^2 - k_{22} \right) + k_{21}^2 \right] \cos^2(2\theta_{d_i}) + k_{22}\omega^2 \cos(4\theta_{d_i})}{\left[\left(k_{11} - \omega^2 \right)^2 + c_{11}^2 \omega^2 \right] \left[\left(k_{22} - \omega^2 \right)^2 + c_{22}^2 \omega^2 \right]}}$$

$$\Psi_i(\omega) = \arctan \left\{ \frac{\begin{array}{l} \omega \left(c_{22} \cos 2\theta_{d_i} - c_{21} \sin 2\theta_{d_i} \right) \left[\left(k_{11} - \omega^2 \right)\left(k_{22} - \omega^2 \right) - c_{11}c_{22}\omega^2 \right] \\ -\omega \left[c_{11} \left(k_{22} - \omega^2 \right) + c_{22} \left(k_{11} - \omega^2 \right) \right] \left[\left(k_{22} - \omega^2 \right) \cos 2\theta_{d_i} + k_{21} \sin 2\theta_{d_i} \right] \end{array}}{\begin{array}{l} \left[\left(k_{22} - \omega^2 \right) \cos(2\theta_{d_i}) + k_{21} \sin(2\theta_{d_i}) \right] \left[\left(k_{11} - \omega^2 \right)\left(k_{22} - \omega^2 \right) - c_{11}c_{22}\omega^2 \right] \\ +\omega^2 \left(c_{22} \cos 2\theta_{d_i} - c_{21} \sin 2\theta_{d_i} \right) \left[c_{11} \left(k_{22} - \omega^2 \right) + c_{22} \left(k_{11} - \omega^2 \right) \right] \end{array}} \right\}$$

Figures

Fig. 1. (a) The structure of the monolithic fused silica cylindrical resonator. **(b)** FEM simulation of the wineglass modes.

Fig. 2. Schematic of: **(a)** the vibration mode of an ideal cylindrical resonator; **(b)** the definition of coordinates and parameters of a practical imperfect cylindrical resonator.

Fig. 3. The experimental setup. The acoustic source excites the cylindrical resonator to the n=2 wineglass mode, and the laser Doppler vibrometer acquires the vibration information, which is then processed by the Polytec software. A rotary table was used to adjust the excitation angle.

Fig. 4. The measurement procedures. **(a)** Seventy-two measurement points were defined equi-angularly on the bottom plate of the resonator, and the excitation was aligned with principle frequency axis. **(b)** The mode shape was identified, and the antinode of the vibration sought out and defined as the zero-degree datum. **(c)** The AFR of each measurement point was fitted in the Polytec software and the Q factor was calculated.

Fig. 5. Experimental results. **(a)** The vibration patterns showed the resonator vibrated at n=2 wineglass mode, and the vibration had a tendency to drift toward the principle axes. **(b)** The circumferential frequency variation. **(c)** The circumferential

Q factor variation when excited at 0° and 5°. **(d)** The circumferential Q factor variation when excited at 10° and 15°.

Fig. 6. Schematic of the two-dimensional oscillator model.

Fig. 7. The exemplification of data collecting and fitting processes. The calculated CB_4 was discretized and then fitted with a single degree-of-freedom damped oscillator model.

Fig. 8. The comparison between numerically simulated Q factors and measured Q factors, when resonator was excited at **(a)** 0°, **(b)** 5°, **(c)** 10°, and **(d)** 15°.

Fig. 9. The comparison between numerically simulated frequencies and measured frequencies, when resonator was excited at **(a)** 10° and **(b)** 15°.